JTTEE5 17:948–955
DOI: 10.1007/s11666-008-9261-6
1059-9630/$19.00 © ASM International

Influence of the Spray Angle on the Characteristics of Atmospheric Plasma Sprayed Hard Material Based Coatings

Wolfgang Tillmann, Evelina Vogli, and Benjamin Krebs

(Submitted May 15, 2008; in revised form September 16, 2008)

This paper presents an investigation of the influence of the spray angle on thermally sprayed coatings. Spray beads were manufactured with different spray angles between 90 and 20° by means of atmospheric plasma spraying (APS) on heat-treated mild steel (1.0503). WC-12Co and Cr_3C_2-10(Ni20Cr) powders were employed as feedstock materials. Every spray bead was characterized by a Gaussian fit. This opens the opportunity to analyze the influence of the spray angle on coating properties. Furthermore, metallographic studies of the surface roughness, porosity, hardness, and morphology were carried out and the deposition efficiency as well as the tensile strength was measured. The thermally sprayed coatings show a clear dependence on the spray angle. A decrease in spray angle changes the thickness, width, and form of the spray beads. The coatings become rougher and their quality decreases.

Keywords Cr_3C_2-NiCr, hard material, morphology, off-axis, spray angle, thermal spraying, WC-12Co

1. Introduction

Sculptured sheets in the automotive industry require forming tools that are able to meet highest demands regarding shape accuracy, even at high complexities, in particular for high-strength steels. These demands are influenced by many uncontrollable variables and partly insufficiently investigated boundary conditions like metallurgical phenomena and tribological effects (Ref 1).

A commonly used process for forming of metal sheets is deep drawing. In recent years, the requirements for the productivity of deep drawing tools have particularly increased in the field of the automotive industry. At the same time, the application of high strength steels has increased due to their potential in the fields of light weight design and advancement in strength (Ref 2). During the forming process of high strength steels enormous press capacities operate, which significantly lead to tool wear. Therefore, it is becoming more and more important to enhance the wear resistance of deep drawing tools by an appropriate surface modification (Ref 3).

A novel approach to surface modification of deep drawing tools is the thermal spraying technology. However, thermally sprayed coatings normally feature undesirable properties like high porosity and roughness especially on complex geometries. In recent years, the complexity of deep drawing tools has highly increased. Consequently, it is often not possible to realize a perpendicular spray angle on the whole component surface during the spray process (Fig. 1). This can lead to significant changes of the coating properties (Ref 4-7). Therefore, it is of high importance to study the influence of the spray angle on the coating properties. This can provide fundamentals to determine the tolerance to which coatings exhibit reproducible properties.

In the present study, experiments have been conducted to investigate the angular dependence of the spray profile, roughness, porosity, hardness, morphology, tensile strength and deposition efficiency of two hard materials in an atmospheric plasma spray process.

2. Experimental

2.1 Substrate Preparation

Rectangular heat-treated mild steel substrates (1.0503) with a dimension of 200 × 100 × 5 mm^3 were employed as base material. The substrates were cut from sheet material. In preparation for thermal spray experiments, the substrates were grit-blasted with coarse-grained alumina (ø = 1180-1700 μm), at a pressure of 4 bar, an

This article is an invited paper selected from presentations at the 2008 International Thermal Spray Conference and has been expanded from the original presentation. It is simultaneously published in *Thermal Spray Crossing Borders, Proceedings of the 2008 International Thermal Spray Conference*, Maastricht, The Netherlands, June 2-4, 2008, Basil R. Marple, Margaret M. Hyland, Yuk-Chiu Lau, Chang-Jiu Li, Rogerio S. Lima, and Ghislain Montavon, Ed., ASM International, Materials Park, OH, 2008.

Wolfgang Tillmann, Evelina Vogli, and **Benjamin Krebs**, Institute of Materials Engineering, Technical University of Dortmund, Leonhard-Euler-Str. 2, 44227, Dortmund, Germany. Contact e-mail: wolfgang.tillmann@udo.edu.

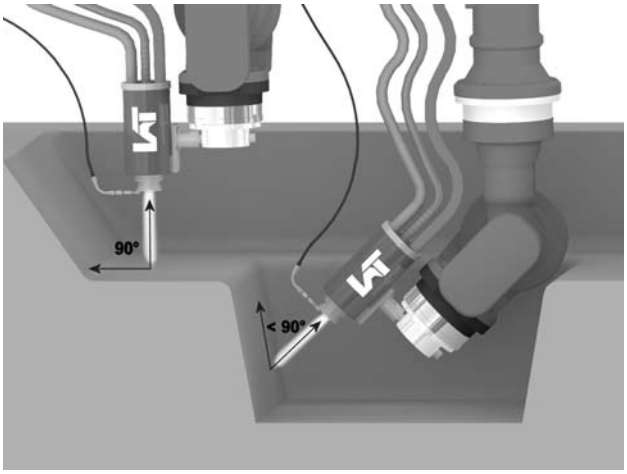

Fig. 1 Scheme of a thermal spray process of a deep drawing tool. Some regions with a high geometrical complexity cannot be coated with a perpendicular spray angle

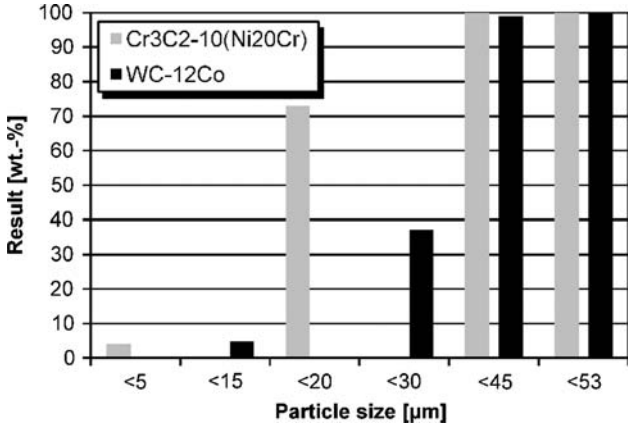

Fig. 2 Cumulative particle size distribution of WC-12Co and Cr_3C_2-10(Ni20Cr) powders

inclination angle of 45°, and a distance of 100 mm. The substrates showed an average roughness R_Z of 50 µm after grit blasting. Afterward, the samples were cleaned in an ethanol ultrasonic bath (15 min) and heated in a furnace (30 min) to approx. 100 °C.

2.2 Feedstock Powder

Two commercially available powders, a WC-12Co (Sulzer Metco, Metco 72F-NS) powder and a Cr_3C_2-10(Ni20Cr) (Sulzer Metco, AMDRY 367) powder, were employed as plasma spray feedstocks. The particle size distribution of the powders was measured by means of laser scattering. The WC-12Co powder possesses particle sizes of 15 to 45 µm with a mode of 30 µm, the Cr_3C_2-10(Ni20Cr) powder below 45 µm with a mode of 20 µm. Their cumulative particle size distribution is shown in Fig. 2. The WC-12Co powder was manufactured by an agglomeration and sintering process and shows a spheroidal shape (Fig. 3a). The Cr_3C_2-10(Ni20Cr) powder was spattered and broken and exhibits a blended shape (Fig. 3b). The chemical composition was measured by inductive coupled plasma—mass spectroscopy (ICP-MS) (Co, Fe, Ni, Cr), the difference method (W), and gravimetry (C). The results are shown in Table 1.

2.3 Experimental Setup

The deposits were manufactured using atmospheric plasma spray equipment Sulzer Metco, model Multi Coat equipped with a F4-MB torch. The main spray parameters are listed in Table 2. The plasma gun moved at a velocity of 0.5 ms^{-1} for 60 overruns accomplished in front of each substrate. The distance between the spray gun and substrate was 130 mm. To prevent overheating of the substrates, the specimens were cooled from the backside with compressed air with a pressure of 2.76 bar.

The experimental setup is shown in Fig. 4. A spray procedure was performed by moving the spray gun horizontally over the substrate. This results in a spray bead in the middle of the substrate. The substrates were coated with spray angles between 90 and 20°. The spray angle is defined as 90° when the spray jet is parallel to the substrate normal and 0° when the jet is perpendicular to the normal. Directly after each coating procedure the temperature on the coating surface was measured by pyrometry. The average temperature of the coatings amounted to 70 °C irrespective of the spray angle.

2.4 Analytics

The profile and the roughness of the spray bead were measured with a 3D surface profilometer (Alicona, model Infinite Focus). The topography of the profile was analyzed by scanning across the spray bead (in Fig. 4 into z-direction). The deposition was characterized by the relative deposition efficiency, which is defined as the ratio of weight gain of specimen coated with a spray angle of 90° to the weight gain of specimen coated with shallower spray angles. Cross sections of the coated samples were investigated by light microscopy (Zeiss, Axiophot) and porosity measurements were done by image processing software (Zeiss, Axiovision 4.6). Microhardness measurements were performed by a Vickers indentation with 0.1 kp (0.981 N) (Leco, model M-400). Each indentation was done for 15 s. Tensile stress tests were accomplished according to DIN EN 582 with a tensile testing devise (Mohr & Federhoff). The roughness, porosity, deposition efficiency, and tensile strength measurements were repeated three times, and the mean of the three values including the standard deviation were determined. The microhardness test was repeated five times.

2.5 Theoretical Background

The central limit theorem states that a sum of n independent, identically distributed random variables at the limit ($n \rightarrow \infty$) can be described by a continuous probability density function, the normal or Gaussian distribution (Ref 8). According to this, a random variable is normally distributed when it is developed from an interaction of a

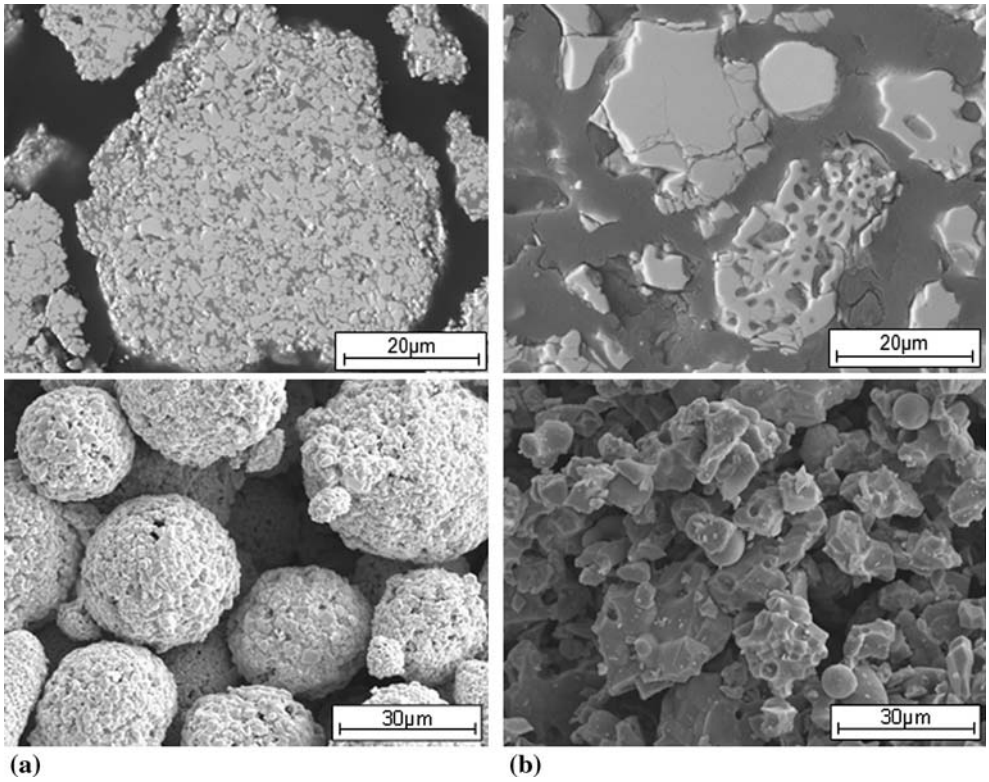

Fig. 3 SEM images of morphology and polished cross section of employed spray powders (a) WC-12Co and (b) Cr_3C_2-10(Ni20Cr)

Table 1 Chemical composition of investigated powders

		Cr_3C_2-10(Ni20Cr)	
[wt.%]	WC-12Co	Cr_3C_2	Ni-20Cr
W	81.52	···	···
Co	12.07	···	···
C	6.15	13.57	···
Ni	···	···	78.40
Cr	···	86.22	20.02

Table 2 Spray parameters

Powder	WC-12Co	Cr_3C_2-10(Ni20Cr)
Plasma gun	F4-MB	F4-MB
Argon flow rate	65 L min^{-1}	65 L min^{-1}
Hydrogen flow rate	7 L min^{-1}	15 L min^{-1}
Current intensity	550 A	550 A
Powder carrier gas flow rate	3.2 L min^{-1}	3.2 L min^{-1}
Powder feed rate	37 g min^{-1}	28 g min^{-1}

large number of influences and the separate influencing value only delivers a minor contribution (e.g., particle impact during thermal spraying). A summation of the separate influencing values is the normal or Gaussian distribution. Many terms of science and engineering such as the spray jet during thermal spraying and the resulting coating profile can be described exactly or in good approximation by this distribution (Ref 9). The mathematical description of the Gaussian distribution is:

$$G(x) := y_0 + \frac{A}{\sigma\sqrt{2\pi}} \cdot \exp\left[-\frac{1}{2}\left(\frac{x - x_0}{\sigma}\right)^2\right] \quad \text{(Eq 1)}$$

where A is an amplitude scale factor, σ is the standard deviation, x_0 the mean, and y_0 an additive constant. The characteristic bell shape of a normal distribution is shown in Fig. 5. The deviation between an experimental measured distribution and the ideal norm distribution is mathematically determined by the skewness s, the kurtosis k, and the full width at half maximum FWHM. The

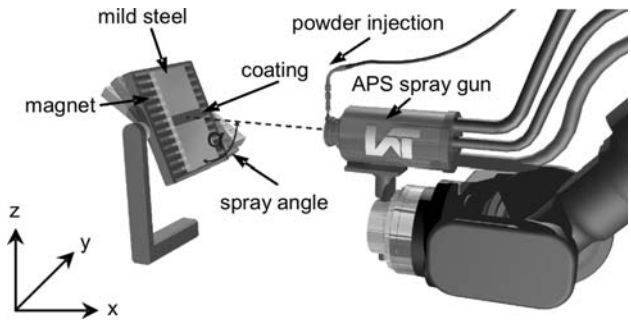

Fig. 4 Scheme of a spray procedure

skewness s is a measure of the symmetry of a distribution in reference to the mean. The skewness can be used to declare if a distribution is concentrated more on the left ($s < 0$) or on the right ($s > 0$) side. The kurtosis k indicates whether a distribution features a higher ($k > 0$) or

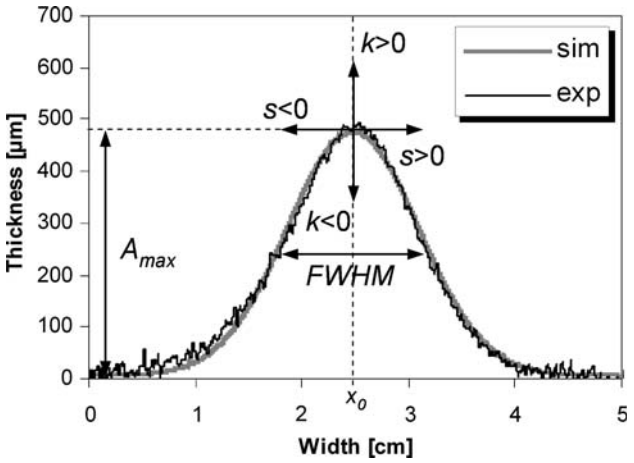

Fig. 5 Experimentally measured Gaussian profile and fit (WC-12Co, $\alpha = 90°$). The profile can be described by the skewness s, the kurtosis k, the full width at half scale FWHM, the mean x_0, and the maximal coating thickness A_{max}

lower ($k < 0$) peakness regarding the normal distribution. The full width at half maximum FWHM is defined as the distance between two abscissa values, where the ordinate values decreased to half of the distribution's maximum. The full width at half maximum is proportional to the standard deviation σ.

3. Results and Discussion

3.1 Topography of the Spray Bead

The spray beads generated at spray angles between 90 and 20° exhibit Gaussian profiles (Fig. 6). For investigation of the profiles Gaussian fits as stated in paragraph 2.5 were used and the relevant parameters, maximal thickness, full width at half maximum, skewness, and kurtosis, were calculated. The maximal thickness A_{max} of the profile increases between 90 and 80° (Fig. 7). Below 80° the thickness decreases with increasing spray angle for both

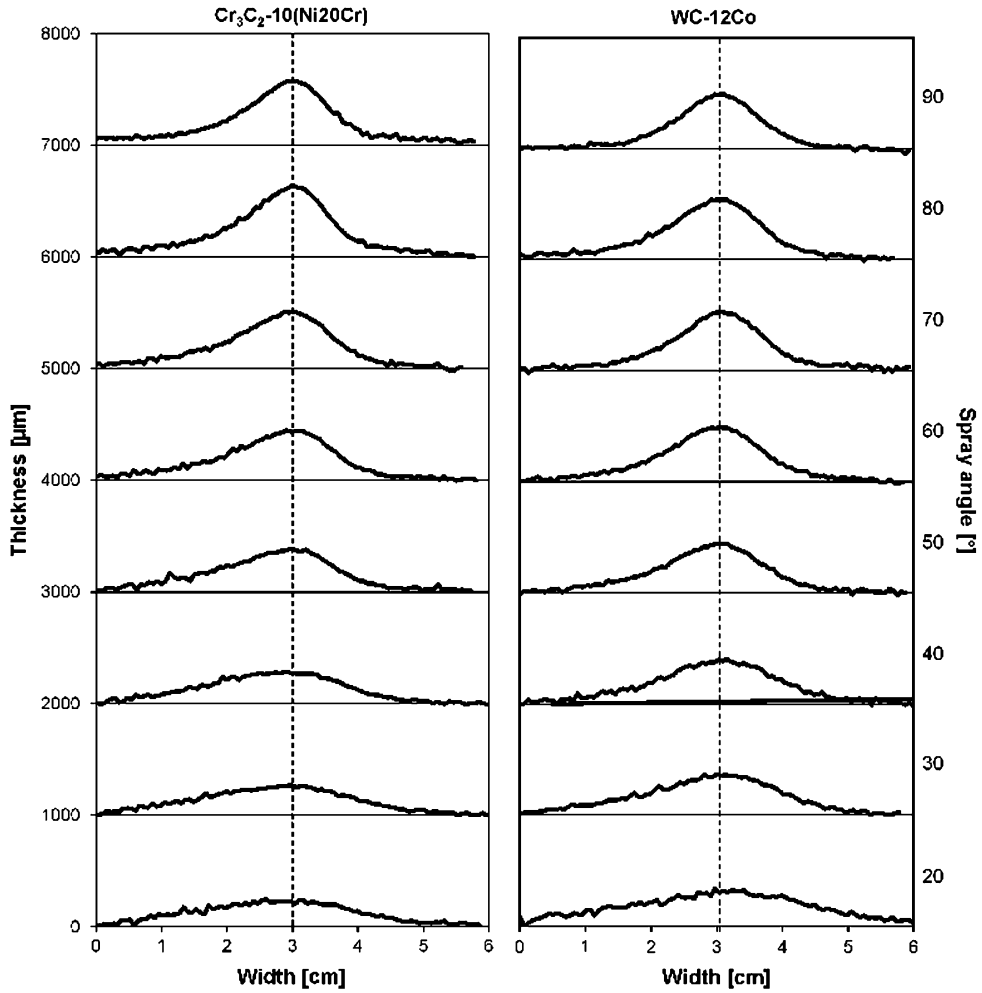

Fig. 6 Topography profiles of WC-12Co and Cr_3C_2-10(Ni20Cr) spray beads made with spray angles between 90 and 20°

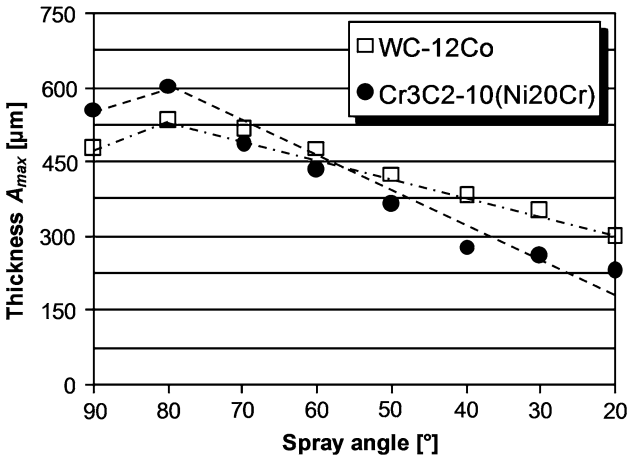

Fig. 7 Thickness A_{max} of spray bead

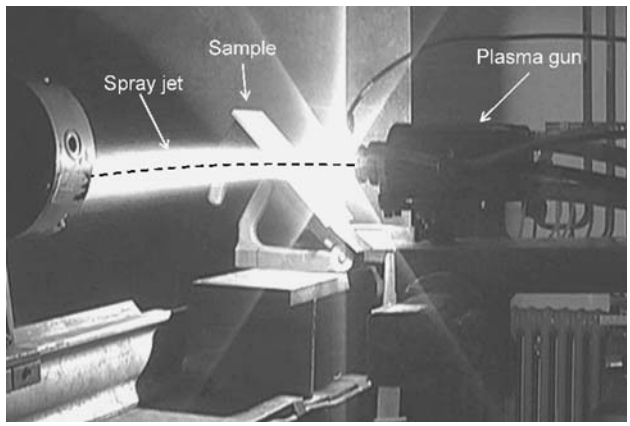

Fig. 8 Experimental setup. The skew spray jet influences the maximal thickness A_{max} of the spray beads and the deposition efficiency DE

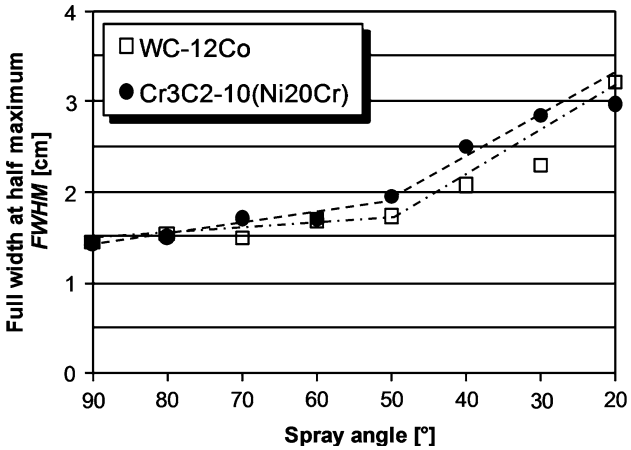

Fig. 9 Full width at half maximum FWHM of spray bead

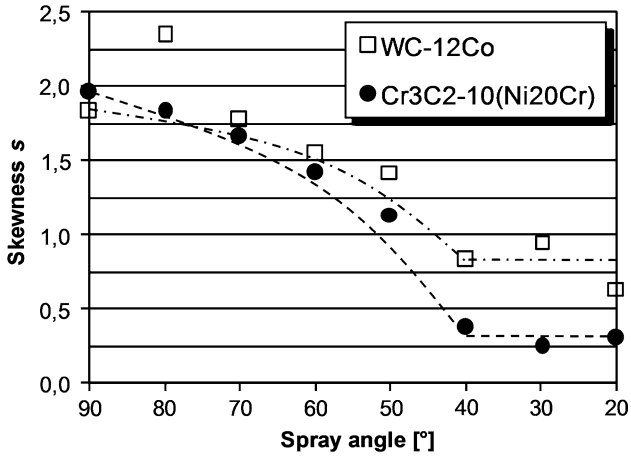

Fig. 10 Skewness s of spray bead

materials. Kang et al. describe the decline in coating thickness at smaller spray angles with a decrease of the normal component of the particle velocity regarding the substrates surface. At the same time the tangential component increases and the probability rises to bounce off a sprayed particle from the specimen's surface. This results in a lower layer thickness (Ref 10). The increase of A_{max} between 90 and 80° is due to a skew spray jet affected by a perpendicular powder injection (Fig. 8). At 90° the sprayed particles exhibit a tangential component with respect to the substrates surface. This leads to a real spray angle smaller than 90° and an increased probability to bounce off sprayed particles. However, at 80° the skewness of the spray jet regarding the substrates surface is compensated and a smaller amount of particles rebound. Consequently, the maximal thickness A_{max} increases.

The full width at half maximum FWHM increases by decreasing the spray angle for both investigated materials (Fig. 9). A slight increase is established between 90 and 50°, whereas the width of the profile increases steeply below 50°. This behavior is due to a growth of the tangential component regarding the substrates surface when decreasing the spray angle and results in a broadening of the spray bead.

The skewness s of the spray beads (Fig. 10) is positive at a spray angle of 90° for both materials. Between 90 and 40° the skewness decreases relatively steeply. Therefore, the symmetry of the spray bead increases. Below 40° only a slight decrease was observed. A positive skewness states a concentration of the spray bead at its right side (in Fig. 4 bottom). The positive skewness at 90° is caused by the perpendicular powder injection. A rotation of the substrate to smaller spray angles leads to a decrease in skewness as long as the substrate rotates in the direction of the profile's concentration. A rotation in the other direction should result in an increase in skewness. This simple behavior is caused by the geometric parameters at off normal angles (Ref 11). However, there are further influencing values such as interaction between sprayed (hard) material and substrates surface. An evidence is the relative constant skewness at spraying angles less than 40°. If the skewness was only influenced by the geometrical

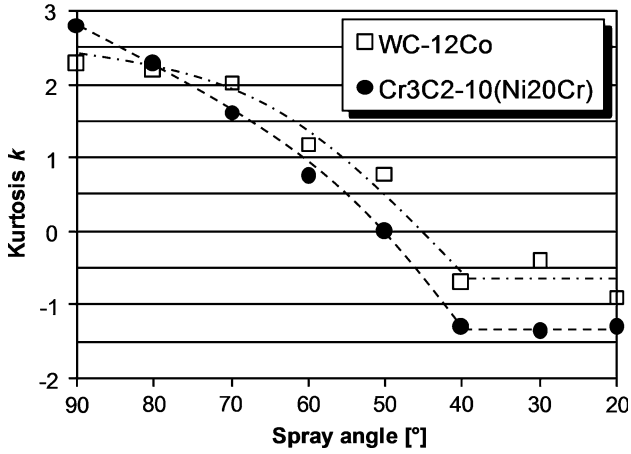

Fig. 11 Kurtosis k of spray bead

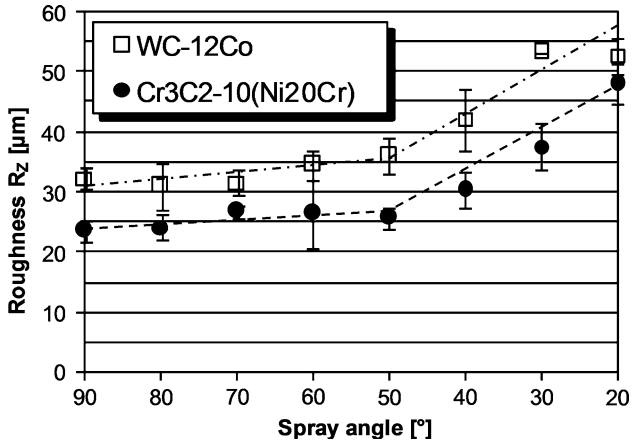

Fig. 12 Surface roughness R_Z versus spray angle

parameters, it should also decrease at small spray angles. The kurtosis k possesses a comparable run as the measured skewness (Fig. 11). At 90° the kurtosis is positive; hence the spray beads show sharp shapes. On reducing the spray angle the kurtosis decreases to negative, and below 40° the kurtosis remains relatively constant. Consequently, the spray bead is broadened and flattened on decreasing the spray angle.

3.2 Roughness

Both spray beads show an increase in the average surface roughness R_Z at decreasing spray angle (Fig. 12). Especially, below 50° the roughness increases steeply. A similar behavior was observed by Smith et al. (Ref 6). This phenomenon is attributed to an increased probability of sprayed particles at low spray angles to interlock with surface inhomogeneities. Consequently, the surface roughness increases.

3.3 Porosity

Within the margin of error the coatings exhibit constant porosities between 90 and 50°. Below 50° a significant

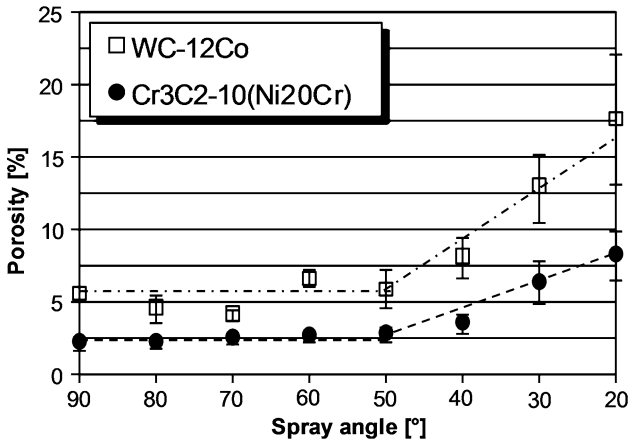

Fig. 13 Porosity versus spray angle

increase of porosity was measured (Fig. 13). Furthermore, the WC-12Co coatings show a more significant tendency to increase in porosity at lower spray angles. An explanation was provided by Smith et al. (Ref 6). Spraying with off normal angles leads to a surface profile with the shape of a sawtooth. Consequently, regions in the sawtooth are shadowed at lower spray angles and therefore striking particles cannot cover the complete surface. As a result pores arise.

The higher porosity and dependency on the spray angle of the WC-12Co coatings compared to the Cr_3C_2-10(Ni20Cr) ones can be explained by the shape, size, and manufacturing method of the employed powder. The WC-12Co powder exhibits a spheroidal shape with a mode of 30 µm, whereas the Cr_3C_2-10(Ni20Cr) is spattered and broken with a mode of 20 µm. Due to the spherical shape of the WC-12Co powder, off normal sprayed particles are likely to slip when they hit the surface. Thus, growing pores are not filled up during spray process. In contrast, it is more likely that a spattered Cr_3C_2-10(Ni20Cr) particle interlocks with the surface of the coating. This can prevent a growth of pores. The lower particle size mode of the Cr_3C_2-10(Ni20Cr) effects smaller spikes at the coating surface and thereby denser coatings. Additionally, the sintered WC-12Co powder possesses a higher porosity than the spattered and broken Cr_3C_2-10(Ni20Cr) powder (cp. Fig. 3). Consequently, the WC-12Co coatings are more porous.

3.4 Relative Deposition Efficiency

The relative deposition efficiency DE increases app. 5% from 90° to 80° (Fig. 14), whereas below 80° the deposition efficiency decreases rather linearly. A decrease in spray angle results in a reduction of the normal component and provides a benefit to the tangential component of the spray particles regarding the substrates surface. An increase in the tangential component results in a higher probability that particles bounce off from the surface of the substrate. Therefore, the deposition efficiency declines. The increase between 90 and 80° is attributed to the perpendicular powder injection into the spray flame. This leads to a skew spray jet with respect to the substrates surface (Fig. 8). The effect is compensated up to 80°.

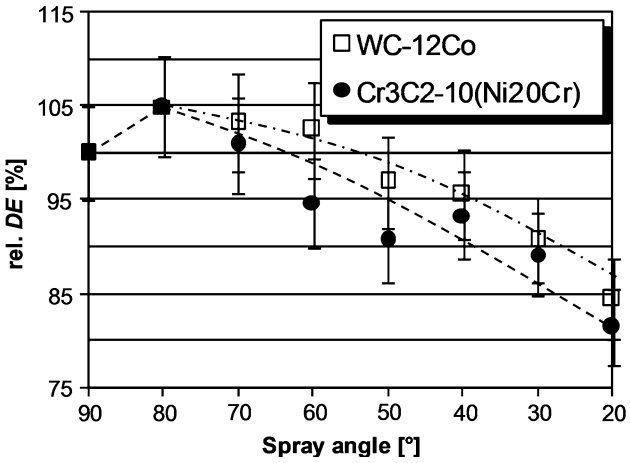

Fig. 14 Variation of relative deposition efficiency with spray angle

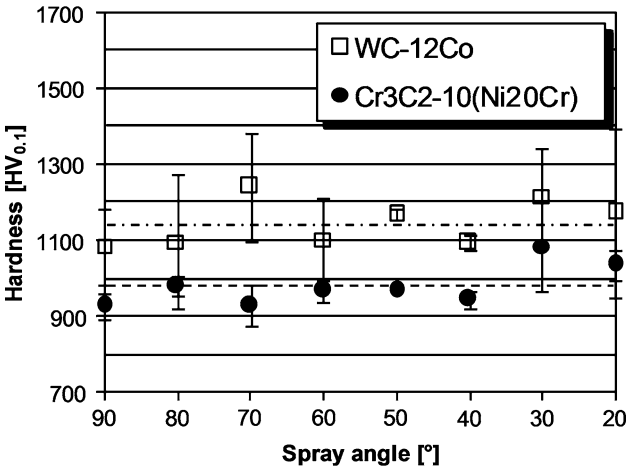

Fig. 15 Relation between microhardness and spray angle

3.5 Hardness

Figure 15 illustrates the results of the microhardness tests. The WC-12Co coatings exhibit hardness between 1080 and 1240$HV_{0.1}$, while Cr_3C_2-10(Ni20Cr) show hardness values between 930 and 1080$HV_{0.1}$. The WC-12Co data points are more widely distributed. This hardness variation is attributed to a more inhomogeneous structure of the coating, which results from the larger powder particle size of the WC-12Co powder. Within the error of margin no dependency of microhardness and spray angle can be stated. The microhardness test affects only small indentations into the coating. Therefore, the influence of pores and changes in microstructure cannot be measured. A macrohardness test should deliver more reliable results.

3.6 Tensile Strength

Figure 16 illustrates the results of the tensile tests. The coatings show a high tensile strength of 67 ± 8 N mm^{-2} for WC-12Co and 65 ± 1 N mm^{-2} for Cr_3C_2-10(Ni20Cr)

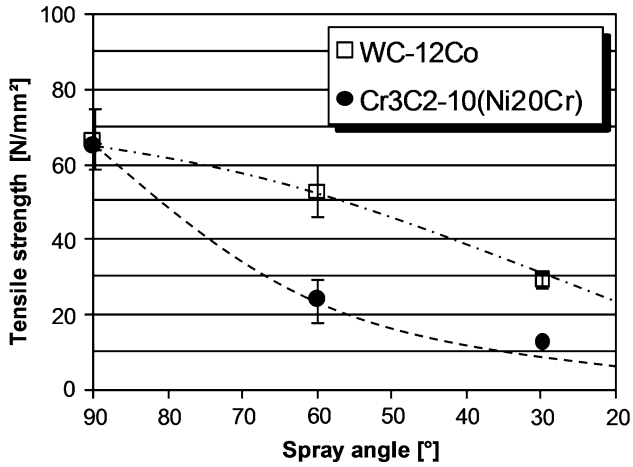

Fig. 16 Effect of spray angle on the tensile strength

at a spray angle of 90°. Both coatings exhibit a significant decrease of the tensile strength on decreasing the spray angle. Particularly, the tensile strength of the WC-12Co coating is strongly influenced by the spray angle.

The coatings sprayed with an angle of 90° delaminated during the tensile tests at the interface between substrate and coating. A decrease in spray angle resulted in an increased probability of a mixed fracture composed of interfacial and cohesive failure. At 30° all coatings failed cohesively. This behavior is due to the rough coating microstructure at smaller spray angles and especially at 30° caused by the high porosity of the coatings.

3.7 Morphology

Polished cross sections of the Cr_3C_2-10(Ni20Cr) and the WC-12Co coatings are illustrated in Fig. 17. The Cr_3C_2-10(Ni20Cr) coatings show a dense structure between 90 and 50°. Below 50° large pores arise. In contrast, the WC-12Co coatings exhibit relative large pores even at 90°. The larger diameter of these pores is due to the particle size of the applied WC-12Co powder. Furthermore, the WC-12Co coating is more sensitive to a change in spray angle. Already at 50° a decline in coating quality is observed.

4. Summary and Conclusion

The results of this study demonstrate that both investigated spray materials show a significant dependence on the spray angle. Independent of the type of powder a change of thickness, width, and profile of the plasma sprayed bead could be established. Especially, from 50° onward the geometry of the spray bead changes considerably. This is connected to an increase in surface roughness and porosity as well as a decrease of tensile strength. The cross sections show a decline in microstructure from 30° for Cr_2C_2-10(Ni20Cr) and from 50° for WC-12Co, whereas a relative linear decrease in deposition efficiency is observed below 80°.

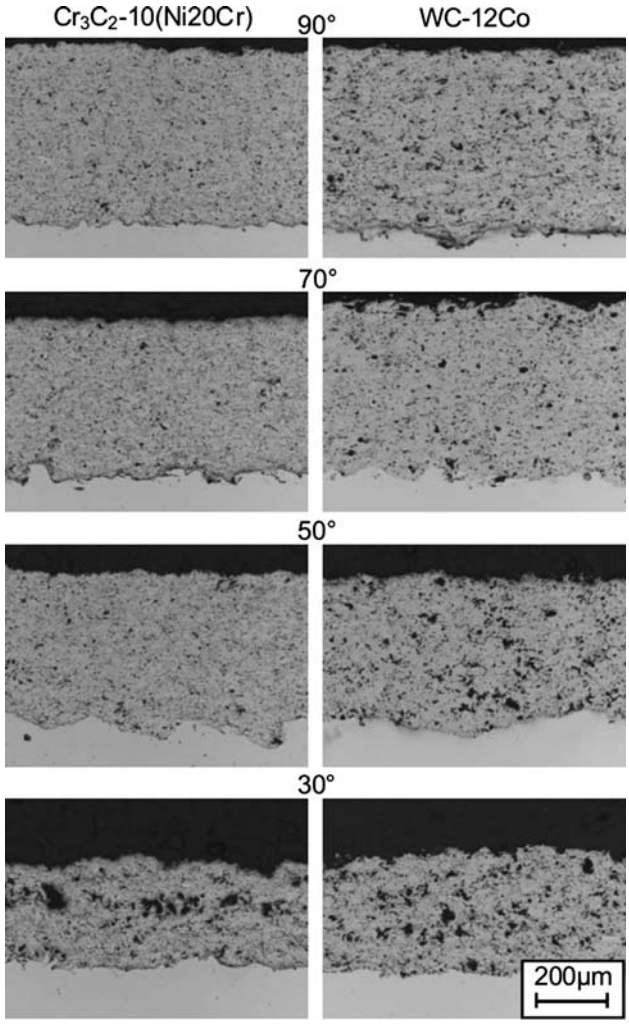

Fig. 17 Cross sections of Cr_3C_2-10(Ni20Cr) and WC-12Co coatings deposited with spray angles between 90 and 30°

Our results suggest that within the traditional 90-45° spray window coatings with only a marginal loss of coating quality can be manufactured. In this window mainly the thickness of the coating and the deposition efficiency decrease. However, for highest shape accuracy the influence of the spray angle must be taken into consideration. Below 45° the coatings show a clear decrease in quality. If possible, these shallow spray angles shall be avoided. If it is not procedurally possible, it must be accepted that the coatings are thinner, with a higher porosity and a higher surface roughness. Only the thickness of the coating can partially be influenced by transferring the spray gun more slowly or numerously over the specimen.

Acknowledgment

This work is supported by the German Research Foundation (DFG) within the Research Centre SFB708.

References

1. A. Hrivnak and L. Sobotova, The Influence of the Deformation Aging and the Conditions of Stress on the Properties of the Deep Drawing Steel Sheet, *J. Mater. Process. Technol.*, 1992, **34**, p 425-130
2. D. Raabe, Werkstücke hoher Qualität und Produktivität durch Verfahrenskombination beim Kaltmassivumformen, *16. Jahrestreffen der Kaltmassivumformer*, Düsseldorf, 2001, p. 1-11
3. H. Schulz-Marner and S. Schulte, Verschleißprüfstand für Blechumformwerkzeuge, *Bänder Bleche Rohre*, 1997, **38**, p 50-53
4. V. Sobolev and J.M. Guilemany, Influence of Droplet Impact Angle on Droplet-substrate Mechanical Interaction in Thermal Spraying, *Mater. Lett.*, 1998, **33**, p 315-319
5. A.J. Allen, G. Long, and H. Herman, Influence of Spray Angle on the Pore and Crack Microstructure of Plasma-Sprayed Deposits, *J. Am. Ceram. Soc.*, 1997, **80**(3), p 733-742
6. M.F. Smith, R.A. Neiser, and R.C. Dykhuizen, An Investigation of the Effects of Droplet Impact Angle in Thermal Spray Deposition, *Proceedings of the 7th National Thermal Spray Conference*, 1994, p. 603-608
7. M.R. Kanouff, R.A. Neiser, and T.J. Roemer, Surface Roughness of Thermal Spray Coating Made with Off-Normal Spray Angles, *J. Therm. Spray Technol.*, 1998, **7**(2), p 219-228
8. L. Sachs, *Angewandte Statistik*, Springer-Verlag, Berlin, 1992, p. 109
9. T. Florin-Iuliu, G. Montavon, and C. Coddet, On the Relationships Between the Geometric Processing Parameters of APS and the Al_2O_3-TiO_2 Deposit Shapes, *Surf. Coat. Technol.*, 2005, **195**, p 54-69
10. C.W. Kang and H.W. Ng, Imaging Diagnostics Study on Obliquely Impacting Plasma-Sprayed Particules Near to the Substrate, *J. Therm. Spray Technol.*, 2006, **15**(1), p 118-130
11. S.H. Leigh and C.C. Berndt, Evaluation of Off-angle Thermal Spray, *Surf. Coat. Technol.*, 1997, **89**, p 213-224